



Cite this: *Chem. Sci.*, 2026, **17**, 1294

All publication charges for this article have been paid for by the Royal Society of Chemistry

Received 6th June 2025  
Accepted 11th November 2025  
DOI: 10.1039/d5sc04158a  
[rsc.li/chemical-science](http://rsc.li/chemical-science)

## Multiple oxidation states of uranium stabilized by an *O,N,O*-ligand

Gabriel J. Juarez,<sup>a</sup> Harris E. Mason,<sup>b</sup> Daniel N. Mangel,<sup>a</sup> Aaron M. Tondreau,<sup>b</sup> and Jonathan L. Sessler<sup>a</sup>

Elements of the 5f row maintain a wide variety of oxidation states that have been exploited in synthesis, catalysis, and separations. Herein, we describe the complexation of an *O,N,O* chelator, ExPh, with uranium in the (IV) and (VI) (uranyl) oxidation states. These two uranium complexes, U(IV)ExPh and UO<sub>2</sub>ExPh, respectively, were characterized in the solid state *via* single-crystal X-ray diffraction (SC-XRD) analysis. Electrochemical studies using cyclic voltammetry were employed to investigate the multiple redox events associated with the U(IV) complex. Spectro-electrochemical analysis of U(IV)ExPh provided spectroscopic evidence of a stable U(V) species. Chemical oxidation of U(IV)ExPh allowed isolation of the U(V) complex, U(V)ExPh. All three stable uranium complexes produced in this study were characterized *via* IR, UV-vis and NMR spectroscopies, and micro-spectrophotometry. On the other hand, efforts to reduce U(IV)ExPh to the corresponding U(III) species or produce this putative complex directly from ExPh failed to yield an isolable product. The stabilization of three formal oxidation states of uranium, coupled with previous lanthanide-row results, paves the way for studies of ExPh and its analogues in minor actinide chemistry.

## Introduction

The use of actinide elements is widespread from medicine to industry, power production, and catalysis.<sup>1–7</sup> Their utility arises not only from prominent radioactivity but also the accessibility of formal oxidation states ranging from (I)–(VII).<sup>8–12</sup> Nevertheless, radiological and heavy element safety concerns, coupled with the unique bonding of the 5f orbitals, has resulted in less understanding of, and notably fewer, actinide complexes relative to their transition and lanthanide counterparts. Within the actinide row, uranium has been the most studied with molecules containing U(I) through U(VI) being reported.<sup>8,13–19</sup> Limited, however, are ligands that have the capacity to complex with uranium in multiple oxidation states.<sup>20,21</sup> Both tri-*s*(aryloxide) and tri-*s*(amide) complexes have been reported to stabilize U(III) and U(IV) through a chemical oxidation with copper.<sup>22</sup> A homoleptic trivalent uranium tetra-amidate complex was also shown to stabilize U(IV) upon chemical oxidation.<sup>23</sup> Recently, a tri-*s*(amido)arene ligand was shown to form complexes with U(II)–U(VI) in a retained framework.<sup>24</sup> An expanded porphyrin, the product of a dedicated synthesis, was also found to stabilize both U(IV) and U(V) complexes.<sup>25</sup> These advances notwithstanding, there remains a need for simple-to-

prepare ligands that display versatility in their uranium coordination chemistry.

Traditional iron-chelators have long been studied as complexes for f-block ions.<sup>26,27</sup> The similarities in charge density, hard-acceptor, Lewis acidity, and interactions with iron-related biological proteins have provided an incentive for such studies.<sup>28–31</sup> While polycarboxylic acids, such as diethylenetriaminepentaacetic acid, were originally studied,<sup>26,30,32</sup> the discovery of biologically produced hydroxamic acid moieties found in bacteria and fungi for iron chelation and transport spearheaded the use of siderophore-type complexants for lanthanide and actinide ion coordination.<sup>32–37</sup> However, of the ligands in question, few have received FDA approval for use as chelators. Medical treatments for contamination or ingestion of actinide ions constitute a need where chelation of radiotoxic nuclides by biocompatible ligands and controlled excretion could prove beneficial.<sup>30,34,38</sup> ExJade is an FDA-approved iron-chelator that has yet to be studied for actinide ion coordination. While ExJade derivatives have shown remarkable therapeutic and sensing capabilities,<sup>39,40</sup> advancing their medicinal utility to encompass radionuclides necessitates investigating their fundamental coordination chemistry with actinide ions. The present study was undertaken as a first step toward achieving this goal.

Previous work in our group established that ExJade analogues, a class of *O,N,O* chelating agents originally developed for the treatment of iron overload disease,<sup>41–43</sup> have an ability to complex with lanthanide ions *via* a low-denticity

<sup>a</sup>Department of Chemistry, The University of Texas at Austin, 105 East 24th Street, Stop A5300, Austin, Texas 78712-1224, USA. E-mail: [sessler@cm.utexas.edu](mailto:sessler@cm.utexas.edu)

<sup>b</sup>Los Alamos National Laboratory, Los Alamos, New Mexico 87544, USA. E-mail: [tondreau\\_a@lanl.gov](mailto:tondreau_a@lanl.gov)



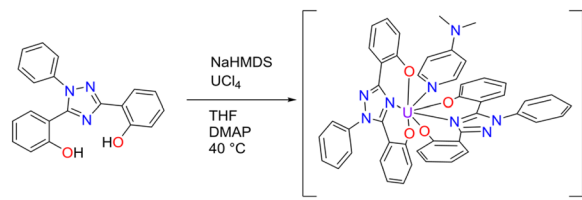
coordination mode.<sup>44</sup> Upon binding, cluster formation and solid precipitation resulted in the separation of Lu(III) from the lighter lanthanides with good selectivity. While the later lanthanide complex formed a multi-metal-centered cluster, the early- and middle-row ions formed as 1 : 1 dimers. These bi-nuclear structural motifs stand in stark contrast to other known f-element ion complexes. While studies of phenolic and nitrogen containing chelators, such as salen-derivatives, have provided insights into uranium complexes in the (IV) or (VI) oxidation states, few have probed the stabilization of a series of oxidation states using the same ligand or the more complicated multi-nuclear or multi-ligand speciation that could result from uranium ion complexation.<sup>45–51</sup> We were thus keen to explore whether ExJade derivatives could (1) stabilize complexes with uranium in various oxidation states, (2) determine the ligand-to-metal stoichiometries, and (3) investigate their associated structural motifs. As detailed below, we have found that a readily accessible ExJade analogue, **ExPh**, supports complex formation with U(IV)–U(VI). Taken in concert, the resulting products not only define a variety of unique coordination motifs but also showcase the versatility of **ExPh** as a ligand capable of supporting uranium complexes in a range of formal oxidation states.

## Results and discussion

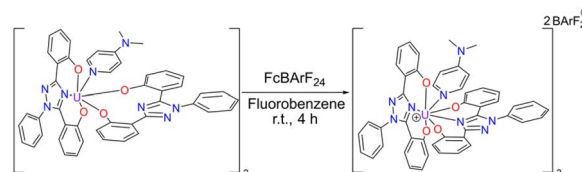
### Synthesis

Pro-ligand **H<sub>2</sub>ExPh** was synthesized as described previously.<sup>40</sup> Initially, a uranyl **ExPh** complex (**UO<sub>2</sub>ExPh**) was synthesized using a protocol analogous to that used to prepare the **ExJade** lanthanide complexes reported earlier.<sup>44</sup> Briefly, under normal atmospheric conditions, uranyl nitrate was added in stoichiometric fashion to a solution of **ExPh** in tetrahydrofuran (THF) containing 2.2 equivalents of triethylamine (TEA) as a base (Scheme 1). Precipitation occurred immediately upon mixing. A minimal amount of dimethylformamide (DMF) was added dropwise until full solubility was achieved. Crystallization of **UO<sub>2</sub>ExPh** occurred directly from the solvent mixture overnight. The isolated yield was 94%.

To obtain the corresponding U(IV) complex, UCl<sub>4</sub> was added to a solution of **ExPh** in THF in an argon-filled dry box in the presence of 2.2 equivalents of sodium bis(trimethylsilyl)amide (HMDS) used as a base (Scheme 2). When precipitation ceased, the reaction was deemed complete. Attempts at crystallization of the U(IV) product produced powders under varying conditions. Therefore, a secondary ligand was added to aid in



Scheme 2 Synthesis of **U(IV)ExPh** under argon in a dry box. The product formed as a 2 : 1 dimer with 4-dimethylaminopyridine (DMAP) as a co-ligand.



Scheme 3 Synthesis of **U(V)ExPh** under argon in a dry box. The dimeric nature of the **U(IV)** starting material is retained in the product.

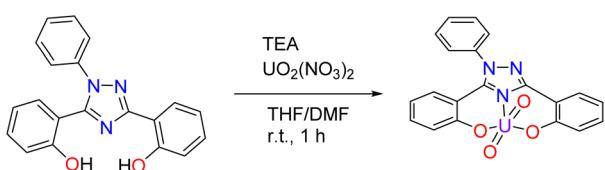
crystallization. Specifically, 1 molar equivalent of 4-dimethylaminopyridine (DMAP) was added to the reaction product to serve as a co-ligand. With the addition of this co-ligand, the product slowly solubilized at elevated temperature. Crystallization was then effected *via* the vapor diffusion of *n*-hexane into the resulting solution at room temperature. This gave **U(IV)ExPh** in 89% yield as a dimeric solid.

Cyclic voltammetry, *vide infra*, was performed on **U(IV)ExPh** to assess the redox chemistry of the complex. To obtain a U(V) complex of **ExPh**, **U(IV)ExPh** was oxidized by treatment with 1 molar equivalent (1 molar equivalents per metal center) of ferrocenium tetrakis(3,5-bis(trifluoromethyl)phenyl)borate (Fc<sup>+</sup>[BarF<sub>24</sub>]<sup>-</sup>) in fluorobenzene to give **U(V)ExPh** (Scheme 3). Initially, the optical characteristics of the solution were reminiscent of the ferrocenium salt. However, a darkening of the solution occurred over the course of the reaction yielding a deep brown product.

Next, attempts were made to prepare the lower oxidation state U(III)-complex. The synthesis was attempted *via* both the stoichiometric incorporation of uranium tris(HMDS) to the pro-ligand **H<sub>2</sub>ExPh** and the chemical reduction of **U(IV)ExPh** with KC<sub>8</sub>. Both procedures resulted in a range of color changes as the reaction chemistry progressed. However, observation and analysis of the resulting equilibrium products, termed **U(III)<sub>red</sub>ExPh** and **U(III)<sub>HMDS</sub>ExPh** for sake of convenience (without implying a successful synthesis), were spectroscopically evocative of the corresponding U(IV) species. On this basis, we conclude that the species in question are either not formed or convert spontaneously to the higher oxidation state U(IV) form. A summary of the uranium chemistry carried out with **ExPh** is provided in Scheme S6.

### Structural characterization

Complexes **U(IV)ExPh** and **UO<sub>2</sub>ExPh** yielded single crystals suitable for single crystal X-ray diffraction (SC-XRD) analysis. In the case of **UO<sub>2</sub>ExPh** the resulting structure revealed formation



Scheme 1 Synthesis of **UO<sub>2</sub>ExPh** performed under normal atmospheric conditions. The product formed as a trimer with a triethylammonium (HTEA) hydroxo-center. A simplified view of the ligand–uranyl complex is shown here.



of a bowl-shaped trimeric complex with a single  $\mu_2$ -oxide from each ligand bridging two uranium metal centers. A central  $\mu_3$ -hydroxo bridge is contained within the trimeric bowl, capped axially by a triethylammonium (HTEA) counter cation (Fig. 1). This uranyl complex stands in contrast to the corresponding early- and middle-row lanthanide structures, which form as 1 : 1 dimeric species. The U–O bond lengths in  $\text{UO}_2\text{ExPh}$  were found to be 2.315(5), 2.227(5), and 2.270(5) Å for the non-bridging phenolates and 2.458(5) and 2.434(5), 2.474(5) and 2.439(5), and 2.457(5) and 2.469(5) Å for the  $\mu_2$ -oxide bridging phenolates. The U–N<sub>triazole</sub> distances were 2.559(5), 2.542(6), and 2.535(6) Å. The uranium-hydroxo bonds were 2.224(5), 2.263(5), and 2.265(5) Å. Twisting of the phenoxide arms resulted in torsion angles between 8.03 and 42.44°. The bending of the triazole core resulted in U–(N–C–N)<sub>triazole</sub> torsion angles between 150.15 and 158.71°.

Solution-state  $^1\text{H}$  NMR spectroscopic studies of  $\text{UO}_2\text{ExPh}$  in  $d_6$ -DMSO revealed the loss of the phenol protons and only a subtle shifting of most peaks from what was seen for the pro-ligand  $\text{H}_2\text{ExPh}$  (Fig. S1 and S2). The three **ExPh** ligands present in  $\text{UO}_2\text{ExPh}$  were found to be in similar chemical environments as inferred from the chemical shift and integration values of key proton peaks. The triethylammonium proton peak was observed at 10.68 ppm, although the integration value was less than expected. This could reflect competition and exchange with the  $d_6$ -DMSO solvent. Due to solubility limitations, corresponding  $^1\text{H}$  NMR spectral analyses were not performed in other solvents. Solution-state  $^{13}\text{C}$  NMR spectral analysis proved concordant with the  $^1\text{H}$  NMR studies in that a similar chemical environment was seen for each **ExPh** unit with non-solvent peaks only within the aromatic region between 110 and 170 ppm.

An SC-XRD analysis of  $\text{U}(\text{iv})\text{ExPh}$  revealed a notable difference in the coordinating ligand framework compared to

$\text{UO}_2\text{ExPh}$ . The crystal formed as a 2 : 1 dimer with one **ExPh** ligand (L1) bridging two uranium centers and one terminal **ExPh** ligand (L2). One DMAP was coordinated to each uranium center yielding  $[[\text{L1L2U}(\text{iv})][\text{DMAP}]]_2 \cdot \text{THF}$  (Fig. 2). Again, a stark contrast to the 1 : 1 dimeric lanthanide complexes was noted. The U–O bond lengths were 2.487(2) Å for the bridging phenolate and 2.164(3) Å for the terminal phenolate of ligand L1. The U–N<sub>triazole</sub> bond length was 2.604(3) Å for L1 *versus* 2.576(3) Å for L2. The U–O bond lengths for L2 were 2.176(3) and 2.276(2) Å. The bridging phenolate of L1 revealed a torsion angle of 39.30° from the plane while the phenolate of L2 had a torsion angle of only 4.99°.

Solution-state  $^1\text{H}$  NMR spectral studies revealed a large paramagnetic shift, between 44.1 and –17.9 ppm, ascribed to pseudo-contact with the coordinated U(iv) metal centers (Fig. S3). Unlike the uranyl complex, each proton in the 2 : 1 structure resulted in a separate peak. To identify the protons within the NMR spectrum, axial and radial  $\chi$  magnetic susceptibility tensors were determined using a pseudo-contact shift (PCS) python algorithm (Fig. 3).<sup>52</sup> The  $\chi$  tensors, structural distances obtained from the crystal data, and pro-ligand  $^1\text{H}$  NMR chemical shifts were then used to predict the paramagnetic chemical shifts (*cf.* SI). For comparison, the magnetic susceptibility of  $\text{U}(\text{iv})\text{ExPh}$  was measured on a magnetic susceptibility balance and found to match well with the predicted value ( $\chi_{\text{iso,atomic}} = 4.34$  *versus*  $4.33 \times 10^{-32} \text{ m}^3$ , respectively). The predictive model was used as a starting point for NMR spectral peak labelling (Table S1).  $^{13}\text{C}$  NMR spectral analyses were also performed; however no usable data could be obtained due to significant line broadening (Fig. S4).

Efforts to obtain single crystals of the proposed di-cationic  $\text{U}(\text{v})$  dimer,  $\text{U}(\text{v})\text{ExPh}$ , proved unsuccessful. As a result, solid-state structural data is limited for this complex. However, a  $^1\text{H}$  NMR spectral analysis ( $d_8$ -THF) revealed significant changes in the chemical shifts of the signals relative to  $\text{U}(\text{iv})\text{ExPh}$  (Fig. S5). The DMAP methyl peaks were still clearly identifiable along with the  $[\text{BArF}_{24}]^-$  counter anion peaks. As

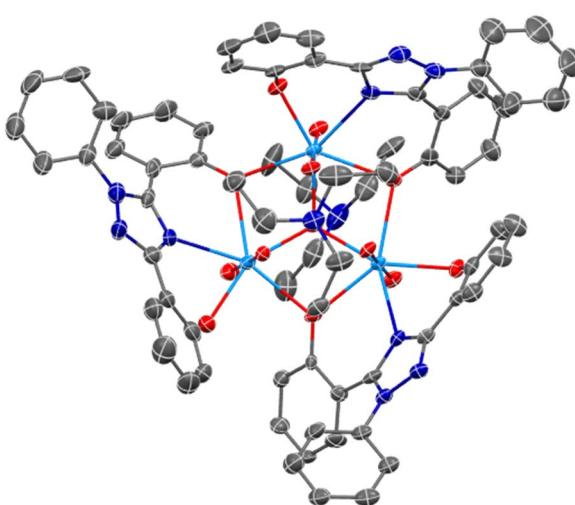


Fig. 1 SC-XRD crystal structure of  $\text{UO}_2\text{ExPh}$  revealing a trimeric, bowl-shaped complex (top-down view). A central hydroxo is contained within the complex that is capped axially by a triethylammonium cation. Ellipsoids are shown at the 50% probability level with hydrogens and solvent molecules omitted for clarity.

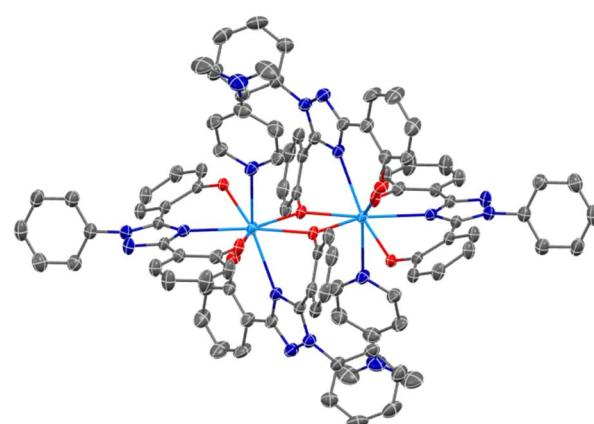


Fig. 2 SC-XRD crystal structure of  $\text{U}(\text{iv})\text{ExPh}$  revealing a dimeric complex containing a  $\mu_2$ -oxide bridge from one phenolate of each monomeric unit. Ellipsoids are shown at the 50% probability level with hydrogens and solvent molecules omitted for clarity.



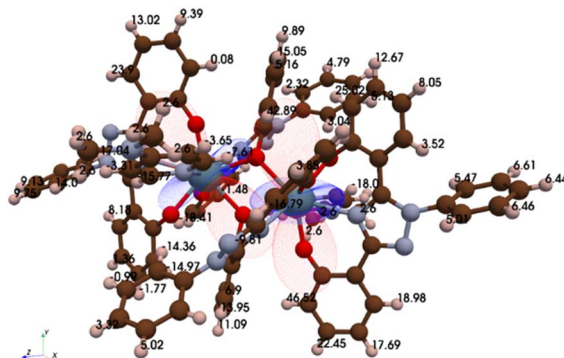


Fig. 3 Results of a modelling study wherein the  $\Delta\chi$  U(iv) tensors are overlaid on the molecular structure. The numbers correspond to the individual calculated chemical shifts for each  $^1\text{H}$  spectral signal (referenced to TMS). The red and blue lobes represent the positive and negative portions of the  $\Delta\chi$  tensor, respectively.

opposed to the U(iv) complex with large paramagnetic shifts, the  $^1\text{H}$  NMR spectrum of **U(v)ExPh** was characterized by chemical shifts within the 17.4 and  $-0.91$  ppm spectral window (Fig. S8). This range is as expected for a U(v) species.<sup>24,53</sup> Nevertheless, in analogy to the U(iv) complex, each proton was considered to reside in a different magnetic environment. The net result was a complicated spectrum whose chemical shift values could not be assigned completely.

The putative U(III) complexes prepared through reduction of the U(iv) form and direct use of an HMDS starting material (*vide supra*) were likewise characterized by  $^1\text{H}$  NMR spectroscopy. The reaction product prepared through reduction gave rise to a spectrum characterized by proton shifts that were nearly identical to those seen for **U(v)ExPh** (Fig. S6). A few of the peaks were shifted; however, this could reflect the presence of free potassium ions arising as a byproduct of the reduction process. The species referred to as **U(III)HMDSExPh** also gave a nearly identical spectrum, except for the clearly identifiable bis(trimethylsilyl) proton peaks (Fig. S7). An overlay of the NMR spectra for **U(v)ExPh** and the products of both attempted preparations of a U(III) form (Fig. S9) highlighted the similarities between the species in question. This correspondence, along with the previous optical spectroscopic findings, leads us to suggest that U(III) **ExPh** complexes are unstable, and, if formed, are transformed readily into the corresponding U(iv) species upon attempted isolation. This presumed instability could be the result of disproportionation of the U(III) centers resulting in generation of the dimeric U(iv) product and a U(II) anionic pair<sup>54–56</sup> or alternatively through alcoholysis of the phenol to yield the U(iv) dimeric complex.<sup>57</sup>

### Electrochemical measurements

An electrochemical study was performed on **U(v)ExPh** to determine the stability of the lower and higher valent uranium species produced upon formal gain or loss of an electron. The experiments were carried out using THF solutions containing 1 mM of the U(iv) complex and 100 mM supporting electrolyte (TBAPF<sub>6</sub>). The open-circuit potential was initially recorded to

determine the equilibrium voltage of the system. Cyclic voltammetry was then performed to assess the accessible oxidation states of the complex. Two irreversible waves were observed for the oxidation, one peak being a smaller pre-wave and the second being a larger irreversible couple (Fig. 4). The pre-wave is thought to reflect a small amount of a monomeric U(iv) complex in solution, which is slightly easier to access electrochemically than the crystallographically characterized 2 : 1 complex. Upon addition of ferrocene, the pre-wave was no longer seen in the oxidative CV scan, while the large anodic peak was characterized by an accelerated onset and substantial broadening (Fig. S29). The ferrocenium reduction wave was also not seen. On the basis of a differential pulse voltammetric analysis (Fig. S30), we conclude that the ferrocene acts as an electron transfer mediator to the U(iv) complex. Thus, following ferrocene oxidation a non-zero steady state current is achieved and only a single oxidation wave is seen. Additional voltammetry experiments were performed in the presence of decamethylferrocene to provide a well-behaved internal reference (Fig. S31). In this case, both the forward and reverse peaks of the iron-reference were observed, along with the pre-waves and oxidation and reduction peaks of the U(iv) complex. Further voltammetric analyses were conducted to elucidate the correlation between the oxidation and reduction peaks seen for the U(iv) complex (*cf.* SI, pp S34 and S35).

As a prelude to the  $\text{Fc}^+[\text{BArF}_{24}]^-$ -based oxidation studies described above, spectro-electrochemical studies were performed on **U(v)ExPh** with the goal of characterizing further the product produced upon oxidation. A potential step from  $-1.0$  to  $1.5$  V was pulsed for 0.5 s. A UV-vis spectrum was taken before and after the potential step. The post-step spectrum revealed the appearance of a broad peak in the visible region between 450 and 650 nm (Fig. S32a). Optical observation of the solution in the cuvette revealed the presence of a deep purple/brown solution shortly after the potential step. Chemical oxidation was then attempted by injecting atmospheric air as a sequence, 0.1 mL aliquots into a cuvette containing 1.5 mL of a 1 mM solution of **U(v)ExPh** in THF. The UV-vis spectra were recorded shortly after each injection and after a final 0.5 mL injection of air. The resulting spectrum proved similar to that seen during

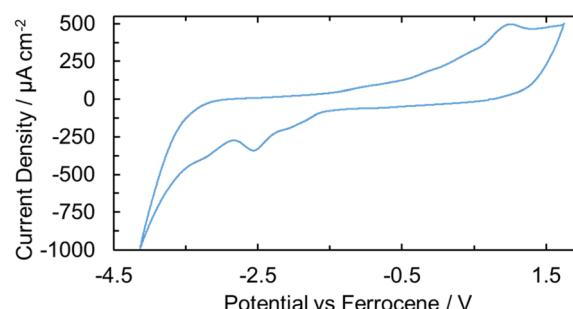


Fig. 4 CV of **U(v)ExPh** as a 1 mM solution in THF containing 100 mM TBAPF<sub>6</sub> as the supporting electrolyte at a scan rate of  $100\text{ mV s}^{-1}$  performed on a glassy carbon electrode. A large, irreversible redox couple is seen at  $E_{\text{pa}} = 1.01\text{ V}$  and  $E_{\text{pc}} = -2.55\text{ V}$ . The large peaks are preceded by two smaller and broader peaks.



the spectro-electrochemical oxidation study (Fig. S32b). The physical appearance of the samples also matched. The apparent ease with which **U(iv)ExPh** underwent both electrochemical and air-based oxidation, led us to consider that a **U(v)** species could be prepared under preparative conditions using ferrocenium as the chemical oxidant as described above.

In contrast to what was seen under conditions of oxidation, a corresponding spectro-electrochemical study revealed no discernible **U(iv)/U(III)** redox events upon reduction. This was taken as further support for the instability of the **U(III) ExPh** complex.

### Solution- and solid-state spectroscopy

The **UO<sub>2</sub>ExPh**, **U(iv)ExPh**, **U(v)ExPh**, and the aspirational **U(III)HMDSExPh** complexes were further analyzed by UV-vis and IR spectroscopies. In the case of the uranyl complex, the UV-vis spectrum revealed a shoulder at 456 nm with a molar absorptivity of  $1420 (\pm 30) \text{ M}^{-1} \text{ cm}^{-1}$  (Fig. S12 and S13). The spectrum for the corresponding **U(v)** complex was characterized by the presence of several peaks at 674, 642, 625, and 545 nm ascribed to f-f transitions. An additional broad peak at 562 nm was also seen that was determined to be non-linear in concentration (Fig. S13). The molar absorptivity values for the linear-in-concentration peaks were determined to be 54 ( $\pm 3$ ), 44 ( $\pm 1$ ), 33.4 ( $\pm 0.3$ ), and  $8 (\pm 2) \text{ M}^{-1} \text{ cm}^{-1}$ , respectively (Fig. S14). A UV-vis spectral analysis of the **U(v)** complex revealed a broad absorption feature between 450 and 650 nm analogous to that observed in the spectro-electrochemical study. An absorption maximum at 474 nm with a molar absorptivity of  $2920 (\pm 450) \text{ M}^{-1} \text{ cm}^{-1}$  was seen (Fig. 5). The deep coloration of **U(v) ExPh** is ascribed to this broad absorption feature, which has been observed previously in various reported **U(v)** complexes.<sup>24,58-61</sup>

The putative **U(III)** complexes displayed a small peak at 607 nm in the UV-vis spectrum that proved non-linear with concentration, as well as a broad peak at 672 nm with a molar absorptivity of  $100 (\pm 30) \text{ M}^{-1} \text{ cm}^{-1}$  (Fig. S17). The similarity of this spectrum and that recorded for **U(iv)ExPh** was taken as further support for the conclusion that the **ExPh** ligand does not stabilize a **U(III)** center effectively, and that if produced, the low-

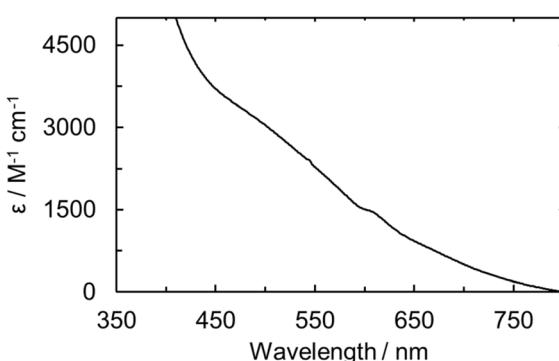


Fig. 5 UV-vis of **U(v)ExPh** measured in fluorobenzene at room temperature. A broad shoulder is observed with maximum at wavelength of 474 nm and a sharper peak at 610 nm.

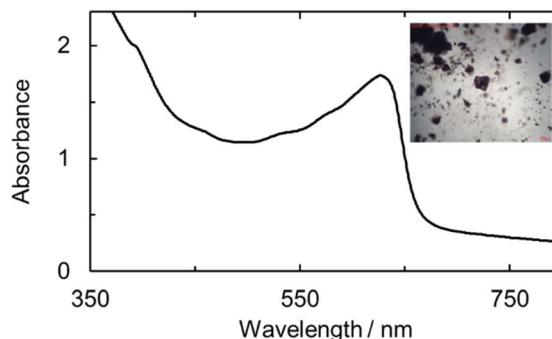


Fig. 6 Micro-spectro photograph of **U(v)ExPh** obtained from crystallized material. A broad shoulder is seen at 394 nm with a sharp peak at 629 nm complementing the solution-state UV-vis spectrum. The inset shows an image of the deep brown/purple plate crystals used for the spectroscopic analysis. Twinning and desolvation is revealed by the several fractures among the crystals.

valent species converts readily to the corresponding **U(iv)** complex. Solution-state NIR spectra revealed no discernible features between the uranyl, **U(iv)**, and putative **U(III)** complexes. The lack of distinction from baseline is ascribed to the poor solubility of the complexes and inability to obtain concentrations necessary for analysis. Solution-state near infrared spectroscopy of the **U(v)** complex revealed a characteristic  $5f^1$  absorption peak. Specifically, a single sharp peak was noted at 1444 nm, consistent with expectations for a **U(v)** complex (Fig. S16).<sup>24,58,62-64</sup>

The purified uranyl, **U(iv)**, and **U(v)** complexes were studied spectroscopically in the solid state using microspectrophotometry (Fig. 6, and S21–S23). Each spectrum revealed absorption features similar in shape and wavelength maximum to the corresponding solution-state spectra, albeit with slight red-shifts.

Solid-state IR data were also obtained for the uranyl, **U(iv)**, **U(v)** and putative **U(III)** complex, (Fig. S18–S20) revealing aromatic C–H and C=C stretches. The triethylammonium and hydroxy groups of **UO<sub>2</sub>ExPh** showed N–H and O–H stretches in the form of a broad peak around  $3400 \text{ cm}^{-1}$ . **UO<sub>2</sub>ExPh**, **U(iv) ExPh**, and the putative **U(III)HMDSExPh** complex showed alkyl C–H stretching modes around  $2950 \text{ cm}^{-1}$  ascribed to their counterions and co-ligands – triethylammonium, DMAP, and HMDS, respectively. A unique  $[\text{BArF}_2]^-$  C–F stretching mode was also observed for the **U(v)ExPh** complex at  $1110 \text{ cm}$  and  $670 \text{ cm}^{-1}$ ; these features were not seen for the other complexes.

## Conclusions

In this study we show that the simple-to-prepare ligand, **ExPh**, recently found effective in lanthanide cation complexation, can stabilize crystallographically characterized complexes with uranium as **U(iv)** and **U(vi)** (uranyl). Electrochemical studies of the **U(iv)** complex, **U(iv)ExPh**, provided support for the conclusion that oxidation to a stable **U(v)** complex could be achieved. Consistent with this supposition, treatment of **U(iv)ExPh** with ferrocenium tetrakis(3,5-bis(trifluoromethyl)phenyl)borate

afforded **U(v)ExPh**. In addition to SC-XRD structural analyses of single crystals of the U(iv) and U(vi) complexes, the three stable products of this study, namely **U(iv)ExPh**, **U(v)ExPh**, and **UO<sub>2</sub>-ExPh**, were characterized in the solid state by IR spectroscopy and micro-spectrophotometry, as well as in solution by <sup>1</sup>H NMR spectroscopy. Efforts were made to prepare the corresponding U(III) species. However, a combination of electrochemical and chemical studies revealed no sign that a stable species was formed. We thus conclude that **ExPh** as a ligand system is not able to stabilize a U(III) metal complex. Nevertheless, the ability to coordinate with uranium cations in three separate formal oxidation states, namely U(IV), U(V), and U(VI), highlights the efficacy of this *O,N,O* chelator toward actinide complexation. This is expected to pave the way for future studies involving transuranic ion chelation, as well as in due course biological evaluations of *inter alia* safety and pharmacokinetic parameters.

## Author contributions

This work was conceived and executed at both the Los Alamos National Laboratory (LANL) and The University of Texas at Austin (UTA) by all authors. G. J. J. and D. N. M. conducted the synthetic work. Formal data analysis of PCS studies were performed by H. E. M. Structural data collection and refinement was carried out by A. M. T. Manuscript preparation and revisions were made by G. J. J., A. M. T., and J. L. S.

## Conflicts of interest

There are no conflicts to declare.

## Data availability

Supplementary information: experimental, photographs of compounds, characterization spectra, details regarding the pseudo-contact shift modelling, and crystallographic data (CIF) for all complexes. The code used for pseudo-contact shift determinations will be provided by A. M. T. upon request. See DOI: <https://doi.org/10.1039/d5sc04158a>.

CCDC 2445901 and 2445902 contain the supplementary crystallographic data for this paper.<sup>65a,b</sup>

## Acknowledgements

Funding at LANL was provided by: Laboratory Directed Research and Development program of LANL under project 2019057ECR, and the Seaborg Institute and a Summer Research Fellowships awarded to GJJ. Funding from the U.S. Department of Energy Office of Basic Energy Sciences Heavy Element Chemistry program (2020LANL372, DE-AC52-06NA25396 to A. M. T.) and Separations program (DE-SC0024393 to J. L. S.) allowed completion of this work and provided support for the ongoing collaboration between A. M. T. and J. L. S.

## Notes and references

1 J. Veliseck-Carolan, *J. Hazard. Mater.*, 2016, **318**, 266.

- B. M. T. Costa Peluzo and E. Kraka, *Int. J. Mol. Sci.*, 2022, **23**, 4655.
- F. A. Settle, *J. Chem. Educ.*, 2009, **86**, 316.
- National Academy of Sciences, *Medical Isotope Production Without Highly Enriched Uranium*, The National Academies Press, Washington D.C., 2009.
- A. R. Fox, S. C. Bart, K. Meyer and C. C. Cummins, *Nature*, 2008, **455**, 341.
- D. R. Hartline and K. Meyer, *JACS Au*, 2021, **1**, 698.
- S. H. Taylor, C. S. Heneghan, G. J. Hutchings and I. D. Hudson, *Catal. Today*, 2000, **59**, 249.
- L. Barluzzi, S. R. Giblin, A. Mansikkamaki and R. A. Layfield, *J. Am. Chem. Soc.*, 2022, **144**, 18229.
- N. B. Mikheev, *Inorg. Chim. Acta*, 1984, **94**, 241.
- B. Ao, H. Lu, Z. Yang, R. Qiu and S. X. Hu, *Phys. Chem. Chem. Phys.*, 2019, **21**, 4732.
- N. B. Mikheev, V. I. Spitsyn, G. V. Ionova and L. N. Auerman, *Radiochim. Acta*, 1984, **37**, 181.
- J. J. Katz, G. T. Seaborg, and L. R. Morss, *The Chemistry of the Actinide Elements*, 2nd edn, Chapman and Hall, London, NY, 1986.
- M. R. MacDonald, M. E. Fieser, J. E. Bates, J. W. Ziller, F. Furche and W. J. Evans, *J. Am. Chem. Soc.*, 2013, **135**, 13310.
- D. R. Kindra and W. J. Evans, *Chem. Rev.*, 2014, **114**, 8865.
- B. Kosog, H. S. La Pierre, M. A. Denecke, F. W. Heinemann and K. Meyer, *Inorg. Chem.*, 2012, **51**, 7940.
- O. J. Cooper, D. P. Mills, J. McMaster, F. Tuna, E. J. L. McInnes, W. Lewis, A. J. Blake and S. T. Liddle, *Chem.-Eur. J.*, 2013, **19**, 7071.
- J. C. Berthet, M. Nierlich and M. Ephritikhine, *Angew. Chem., Int. Ed.*, 2003, **42**, 1952.
- K. Takao, S. Tushima, T. Ogura, T. Tsubomura and Y. Ikeda, *Inorg. Chem.*, 2014, **53**, 5772.
- M. Ephritikhine, *Organometallics*, 2013, **32**, 2464.
- S. Fortier, N. Kaltsoyannis, G. Wu and T. W. Hayton, *J. Am. Chem. Soc.*, 2011, **133**, 14224.
- D. K. Modder, C. T. Palumbo, I. Douair, F. Fadaei-Tirani, L. Maron and M. Mazzanti, *Angew. Chem., Int. Ed.*, 2021, **60**, 3737.
- R. K. Thomson, C. R. Graves, B. L. Scott and J. L. Kiplinger, *Inorg. Chem. Commun.*, 2011, **14**, 1742.
- M. D. Straub, S. Hohloch, S. G. Minasian and J. Arnold, *Dalton Trans.*, 2018, **47**, 1772.
- C. Deng, J. Liang, R. Sun, Y. Wang, P. X. Fu, B. W. Wang, S. Gao and W. Huang, *Nat. Commun.*, 2023, **14**, 4657.
- J. T. Brewster, D. N. Mangel, A. J. Gaunt, D. P. Saunders, H. Zafar, V. M. Lynch, M. A. Boreen, M. E. Garner, C. A. P. Goodwin, N. S. Settineri, J. Arnold and J. L. Sessler, *J. Am. Chem. Soc.*, 2019, **141**, 17867.
- G. N. Stradling, *J. Alloys Compd.*, 1998, **271**, 72.
- N. C. O'Boyle, G. P. Nicholson, T. J. Piper, D. M. Taylor, D. R. Williams and G. Williams, *Appl. Radiat. Isot.*, 1997, **48**, 183.
- A. K. Sockwell and M. Wetzler, *Chem.-Eur. J.*, 2019, **25**, 2380.
- K. N. Raymond, G. E. Freeman and M. J. Kappel, *Inorg. Chim. Acta*, 1984, **94**, 193.
- S. Fukuda, *Curr. Med. Chem.*, 2005, **12**, 2765.

31 P. Jewula, J. C. Berthet, J. C. Chambron, Y. Rousselin, P. Thuery and M. Meyer, *Eur. J. Inorg. Chem.*, 2015, **2015**, 1529.

32 K. N. Raymond, G. Müller, and B. F. Matzanke, Complexation of iron by siderophores a review of their solution and structural chemistry and biological function, in *Structural Chemistry. Topics in Current Chemistry*, Springer, Berlin, Heidelberg, 1984, vol. 123, p. 49.

33 P. W. Durbin, N. Jeung, S. J. Rodgers, P. N. Turowski, F. L. Weitl, D. L. White and K. N. Raymond, *Radiat. Prot. Dosim.*, 1989, **26**, 351.

34 C. E. Ruggiero, J. H. Matonic, S. D. Reilly and M. P. Neu, *Inorg. Chem.*, 2002, **41**, 3593.

35 A. S. Ivanov, B. F. Parker, Z. Zhang, B. Aguila, Q. Sun, S. Ma, S. Jansone-Popova, J. Arnold, R. T. Mayes, S. Dai, V. S. Bryantsev, L. Rao and I. Popovs, *Nat. Commun.*, 2019, **10**, 819.

36 T. Terencio, J. Roithova, S. brandes, Y. Rousselin, M. J. Penouilh and M. Meyer, *Inorg. Chem.*, 2018, **57**, 1125.

37 A. E. V. Gorden, J. Xu, K. N. Raymond and P. Durbin, *Chem. Rev.*, 2003, **103**, 4207.

38 L. Mullen, C. Gong and K. Czerwinski, *J. Radioanal. Nucl. Chem.*, 2007, **273**, 683.

39 A. C. Sedgwick, K. C. Yan, D. N. Mangel, Y. Shang, A. Steinbrueck, H. H. Han, J. T. Brewster II, X. L. Hu, D. W. Snelson, V. M. Lynch, H. Tian, X. P. He and J. L. Sessler, *J. Am. Chem. Soc.*, 2021, **143**, 1278.

40 A. Steinbrueck, A. C. Sedgwick, S. M. Hwang, S. Sen, M. Y. Zhao, D. Y. Huang, D. M. Knoll, Y. Y. Wang and J. L. Sessler, *Chemosensors*, 2021, **9**, 68.

41 H. Nick, *Curr. Opin. Chem. Biol.*, 2007, **11**, 419.

42 M. D. Cappellini and P. Pattoneri, *Annu. Rev. Med.*, 2009, **60**, 25.

43 R. Galanello, S. Campus and R. Origa, *Expert Opin. Drug Metab. Toxicol.*, 2012, **8**, 123.

44 D. N. Mangel, G. J. Juarez, S. H. Carpenter, A. Steinbrueck, V. M. Lynch, J. Yang, A. C. Sedgwick, A. Tondreau and J. L. Sessler, *J. Am. Chem. Soc.*, 2023, **145**, 22206.

45 E. R. Mikeska, M. Z. Makos, G. A. Arehart, V. A. Glezakou and J. D. Blakemore, *Inorg. Chem.*, 2025, **64**, 5827.

46 M. S. Bharara, K. Heflin, S. Tonks, K. L. Strawbridge and A. E. V. Gorden, *Dalton Trans.*, 2008, 2966.

47 A. Kumar, D. Lionetti, V. W. Day and J. D. Blakemore, *J. Am. Chem. Soc.*, 2020, **142**, 3032.

48 G. Nocton, P. Horeglad, V. Vetere, J. Pecaut, L. Dubois, P. Maldivi, N. M. Edelstein and M. Mazzanti, *J. Am. Chem. Soc.*, 2010, **132**, 495.

49 B. E. Klamm, C. J. Windorff, C. Celis-Barros, M. L. Marsh and T. E. Albrecht-Schmitt, *Inorg. Chem.*, 2020, **59**, 23.

50 R. R. Golwankar, M. Z. Makos, N. Cajiao, M. L. Neidig, A. G. Oliver, C. S. Day, V. W. Day, V. A. Glezakou and J. D. Blakemore, *Inorg. Chem.*, 2024, **63**, 24542.

51 L. Salmon, P. Thuery and M. Ephritikhine, *Dalton Trans.*, 2004, 1635.

52 H. W. Orton, T. Huber and G. Otting, *Magn. Reson.*, 2020, **1**, 1.

53 A. C. Schmidt, F. W. Heinemann, L. Maron and K. Meyer, *Inorg. Chem.*, 2014, **53**, 13142.

54 P. L. Arnold, S. M. Mansell, L. Maron and D. McKay, *Nat. Chem.*, 2012, **4**, 668.

55 P. L. Diaconescu, P. L. Arnold, T. A. Baker, D. J. Mindiola and C. C. Cummins, *J. Am. Chem. Soc.*, 2000, **122**, 6108.

56 P. L. Diaconescu and C. C. Cummins, *Inorg. Chem.*, 2012, **51**, 2902.

57 D. L. Clark, A. P. Sattelberger, W. G. Van Der Sluys and J. G. Watkin, *J. Alloys Compd.*, 1992, **180**, 303.

58 C. R. Graves, P. Yang, S. A. Kozimor, A. E. Vaughn, D. L. Clark, S. D. Conradson, E. J. Schelter, B. L. Scott, J. D. Thompson, P. J. Hay, D. E. Morris and J. L. Kiplinger, *J. Am. Chem. Soc.*, 2008, **130**, 5272.

59 A. M. Tondreau, T. J. Duignan, B. W. Stein, V. E. Fleischauer, J. Autschbach, E. R. Batista, J. M. Boncella, M. G. Ferrier, S. A. Kozimor, V. Mocko, M. L. Neidig, S. K. Cary and P. Yang, *Inorg. Chem.*, 2018, **57**, 8106.

60 S. T. Loffler, J. Hummer, A. Scheurer, F. W. Heinemann and K. Meyer, *Chem. Sci.*, 2022, **13**, 11341.

61 G. Kniewald and M. Branica, *Mar. Chem.*, 1988, **24**, 1.

62 X. Xin, I. Douair, T. Rajeshkumar, Y. Zhao, S. Wang, L. Maron and C. Zhu, *Nat. Commun.*, 2022, **13**, 3809.

63 N. H. Anderson, H. Yin, J. J. Kiernicki, P. E. Fanwick, E. J. Schelter and S. C. Bart, *Angew. Chem., Int. Ed.*, 2015, **54**, 9386.

64 N. H. Anderson, S. O. Odoh, Y. Yao, U. J. Williams, B. A. Schaefer, J. J. Kiernicki, A. J. Lewis, M. D. Goshert, P. E. Fanwick, E. J. Schelter, J. R. Walensky, L. Gagliardi and S. C. Bart, *Nat. Chem.*, 2014, **6**, 919.

65 (a) CCDC 2445901: Experimental Crystal Structure Determination, 2025, DOI: [10.5517/ccdc.csd.cc2n3510](https://doi.org/10.5517/ccdc.csd.cc2n3510); (b) CCDC 2445902: Experimental Crystal Structure Determination, 2025, DOI: [10.5517/ccdc.csd.cc2n3521](https://doi.org/10.5517/ccdc.csd.cc2n3521).

